Available online at www.sciencedirect.com
SCIENCE DIRECT®
Journal of Power Sources 135 (2004) 79–87
JOURNAL OF POWER SOURCES
www.elsevier.com/locate/jpowsour

# Predicting water and current distributions in a commercial-size PEMFC

S. Shimpalee [a], S. Greenway [a], D. Spuckler [b], J.W. Van Zee [a,*]

[a] *Department of Chemical Engineering, University of South Carolina, Columbia, SC 29208, USA*
[b] *CD adapco Group, Melville, NY 11747, USA*

Received 13 February 2004; accepted 10 March 2004

Available online 8 June 2004

**Abstract**

Many researchers have experimentally studied small (~10–50 $cm^2$), single cell PEMFC systems to understand the behavior and electrochemistry of PEMFC. Also, three-dimensional electrochemical models have been used to predict the distributions of current, temperature, and species mole fractions as a function of the operating conditions and geometry of small cells and these predictions have been compared with experimental data. However, the commercial viability of PEMFC systems depends on understanding the mass transport and electrochemistry of large-scale electrodes with reacting area on the order of 200–600 $cm^2$ and numerical investigation of PEMFCs of this size have been effectively impossible without the recent advances in parallel computation and processor speed. This paper applies a parallelized three-dimensional computational fluid dynamics (CFD) model to a 480 $cm^2$ PEMFC flow-field selected from US patent literature to demonstrate that analysis of large-scale cells is possible. The distributions of pressure, temperature, and electrochemical variables for stationary and automotive operating conditions are examined. Using parallel computing techniques, the computational time is shown to be significantly reduced by increasing the number of processors while maintaining less than 1% error in mass balance.


*Keywords:* PEM fuel cell; CFD modeling; Parallel computing; STAR-CD; Flow-field design; Water management; Large-scale PEMFC

## 1. Introduction

To a first approximation, the power from proton exchange membrane fuel cells (PEMFC) depends on the number of cells in the stack and the size of the reaction area in each cell. That is to a first approximation the stack voltage is increased by adding cells and the stack current is increased by using larger electrodes. Typically, reaction areas between 200 and 600 $cm^2$ are used in both stationary and automobile applications. Consequently, many engineers are designing and testing gas flow-fields for PEMFCs in this size range. However, only performing experimental studies on commercial-scale cells are inadequate to develop complete flow-field design heuristics and understand the mass transport and electrochemical phenomena occurring in commercial-size plates. Numerical studies that elucidate these physics have to this point been complicated by the large size of the computational domain needed for PEMFC simulations.

In recent numerical studies, most researchers examined local species and electrochemical variable distributions on small-scale PEMFCs. Some of these studies simplified the physics to be isothermal and single phase [1–10] and some of models have been included two-phase behavior of water inside PEMFC to capture the behavior of liquid water caused by condensation [11–15]. However, all of these works focused on model development for small PEMFCs and therefore, the solution convergence including mass balance inspection and geometry's grid optimization are simple to achieve. Some of these works have been reviewed by Shimpalee et al. [16].

The inherent non-linearity of the equations governing PEMFC performance on a three-dimensional level requires iterative solution techniques. Solving a full three-dimensional CFD model for the flow channel and diffusion layers of a PEMFC shows important interactions of porous media and flow-field that affect distributions of current, temperature, and species transport as discussed in Lee et al. [14]. This type of model lends itself well to investigating the physics inside commercial-scale PEMFCs. In this study, the three-dimensional model of Shimpalee and coworkers [13–15] is used with the commercial CFD solver STAR-CD (Version 3.150) by including the parallel computing technique into the solver called STAR-HPC. The computational time is reduced by increasing of the number

* Corresponding author. Tel.: +1-803-777-2285; fax: +1-803-777-8142.
*E-mail address:* vanzee@engr.sc.edu (J.W. Van Zee).

0378-7753/$ – see front matter © 2004 Elsevier B.V. All rights reserved.
doi:10.1016/j.jpowsour.2004.03.059

Table 1
Operating conditions (note that the inlet mole fraction of $H_2$ and $N_2$ is 40 and 60%, respectively, on a dry basis and the mass fractions of $N_2$, $H_2$, $O_2$, and $H_2O$ are described as $m_{N_2}$, $m_{H_2}$, $m_{O_2}$, and $m_{H_2O}$)

| Current density ($A/cm^2$) | Anode properties | | | | Cathode properties | | | |
|---|---|---|---|---|---|---|---|---|
| | Inlet velocity (m/s) | $m_{N_2}$ | $m_{H_2}$ | $m_{H_2O}$ | Inlet Velocity (m/s) | $m_{N_2}$ | $m_{O_2}$ | $m_{H_2O}$ |
| Humidified cathode feed: inlet boundary conditions with 40% $H_2$ and 60% $N_2$, 70 °C/70 °C inlet dew points, 1.2/2.0 stoich, 480 $cm^2$ reaction area | | | | | | | | |
| 0.1 | 1.865 | 0.659 | 0.031 | 0.310 | 2.961 | 0.612 | 0.172 | 0.216 |
| 0.2 | 3.730 | 0.659 | 0.031 | 0.310 | 5.923 | 0.612 | 0.172 | 0.216 |
| 0.6 | 11.191 | 0.659 | 0.031 | 0.310 | 17.768 | 0.612 | 0.172 | 0.216 |
| 0.8 | 14.921 | 0.659 | 0.031 | 0.310 | 23.691 | 0.612 | 0.172 | 0.216 |
| Dry cathode feed: inlet boundary conditions with 40% $H_2$ and 60% $N_2$, 70 °C/bypass inlet dew points, 1.2/2.0 stoich, 480 $cm^2$ reaction area | | | | | | | | |
| 0.1 | 1.865 | 0.659 | 0.031 | 0.310 | 2.058 | 0.780 | 0.220 | 0.000 |
| 0.2 | 3.730 | 0.659 | 0.031 | 0.310 | 4.115 | 0.780 | 0.220 | 0.000 |
| 0.6 | 11.191 | 0.659 | 0.031 | 0.310 | 12.346 | 0.780 | 0.220 | 0.000 |
| 0.8 | 14.921 | 0.659 | 0.031 | 0.310 | 16.461 | 0.780 | 0.220 | 0.000 |

of processors over which a job is divided. The work is the first full commercial-size (480 $cm^2$) three-dimensional PEMFC model study with J.A. Rock patent flow-field design [17]. Consequently, the details of local current density, water, temperature and reacting gas concentrations are investigated. The operating conditions investigated in this study (described below) have been chosen to investigate the effects of current trends in PEMFC operation.

Many PEMFC system manufacturers are investigating drier operating conditions, especially on the cathode, to help alleviate water management issues in PEMFC systems especially in transportation applications [18]. In this work, the effects of dry cathode feed conditions are compared to a well-humidified cathode. The PEMFC system simulated operates with 20% excess hydrogen and 100% excess oxygen at a cell temperature of 70 °C and the run with dilute $H_2$ stream in the anode and air in the cathode. The fuel used here is 40% hydrogen in inert gases and air is modeled as a mixture of only oxygen and nitrogen. This dilution may be a result of accumulation of $N_2$ passed through the membrane electrode assembly (MEA) from the cathode. These results may also be applicable to a stationary application where the inert is a mixture of $CO_2$ and $N_2$ resulting from reforming natural gas. Under humidified cathode conditions, both anode and cathode gases contain enough water vapor to reflect saturation at a 70 °C dew point temperature. Under dry cathode conditions no water vapor is included in the cathode feed while the anode is humidified to saturation at 70 °C dew point temperatures. This simulates having the air inlet bypass the cathode humidifier. Bypassing the cathode humidifier would reduce the burden of water management and the lower pressure drop inside the PEMFC system. Details of the operating conditions and parameters are shown in Tables 1 and 2.

Table 2
Operating parameters

| Model parameters | |
|---|---|
| Permeability of diffusion layer ($\times 10^{12}$ $m^2$) | 1.0 (porosity ~70%) |
| GDL thermal conductivity (W/m K) | 0.213 |
| MEA thermal conductivity (W/m K) | 0.147 |
| Dry membrane density ($g/cm^3$) | 2.0 |
| Equivalent weight of dry membrane (g/mol) | 1100 |
| Anode exchange current density ($A/m^2$) | 5000 |
| Anode transfer coefficient | 1.2 |
| Cathode exchange current density ($A/m^2$) | 500 |
| Cathode transfer coefficient | 0.6 |
| Condensation rate (1/s) | 1.0 |
| Evaporation rate (1/s) | 1.0 |
| Graphite conductivity (W/m K) | 5.7 |
| Open circuit voltage (V) | 0.95 |
| Operating pressure (atm) | 1.0 |

## 2. Model development

This numerical simulation is based on three-dimensional mass transfer model of a commercial-size PEMFC with temperature dependent and water phase change [13–15]. The activities in the membrane are simulated through source terms in the control volumes in contact with the membrane. Note that the Navier–Stokes equations, the species transport equations, the energy equation including a water phase change model, the solubility effect of reacting gas in the water film presented on the MEA surface, and the electrochemical equations are shown in [13–15] and are not repeated here. A control volume technique based on STAR-CD (Version 3.150) commercial flow solver was used to solve the governing equations. Subroutines were added to calculate and account for the source terms, electrochemical reactions, and flux of protons and water across the membrane as also described in [13–15].

Figs. 1 and 2 show the geometry of the fuel cell with flow-field from J.A. Rock's Patent [17] that was modeled in this work. This arrangement consists of two flow channels separated by diffusion layers and MEA and the figure also shows the channel geometry and associated

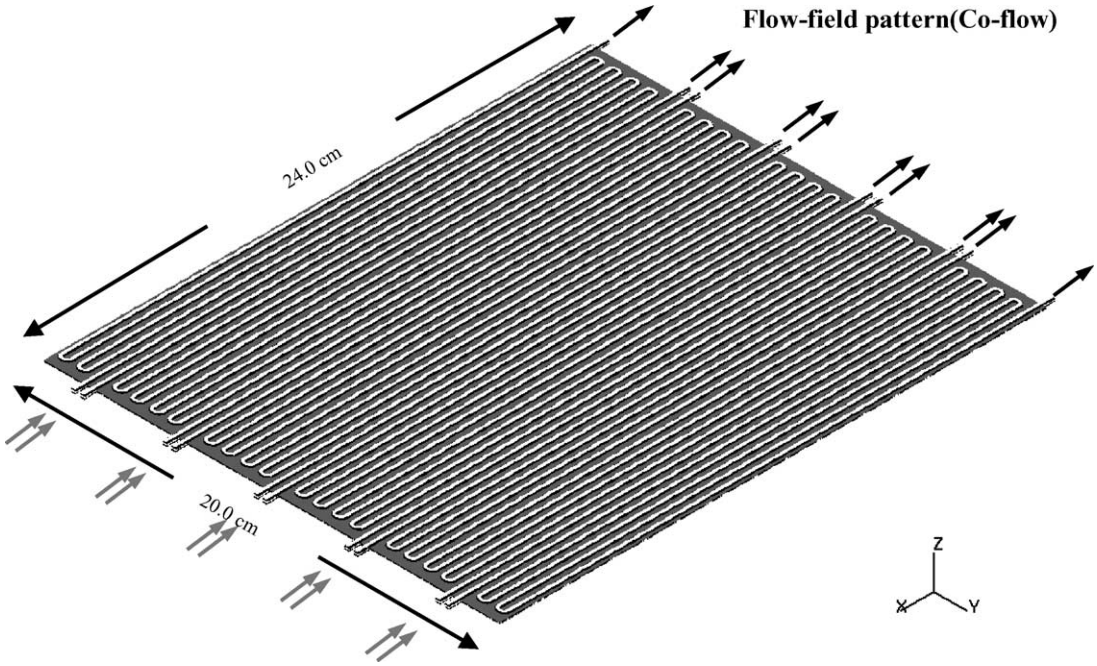


Fig. 1. Four hundred and eighty square centimeter PEMFC with flow-field model geometry without graphite current collector for computational analysis ([17]).

coordinate system. A thin MEA is sandwiched between anode and cathode diffusion layers. Fig. 2 shows the geometrical details of a portion of the computational domain, which consists of the anode flow channel, anode diffusion layer, MEA, cathode diffusion layer, and cathode flow channel. Fig. 2 also demonstrates the trimmed mesh technique used to generate the computational domain which conforms to the physical design of the flow-field. This trimmed mesh technique combines tetrahedrals, prisms, hexahedral, and trimmed cells to account for regions of curvature in the computational domain. There are five serpentine passes in the flow path with 10 symmetric patterns on the 480 $cm^2$ reaction area, so that the flow is approximately 120 cm long in the axial direction with 1.1 $mm^2$ cross-section flow area. Each diffusion layer has dimension of 0.025 (height) × 20.0 (width) × 24.0 (length) $cm^3$. A total of 4,951,440 cells (elements) including graphite current collector were used to model the fuel cell. The transport of water and proton is simulated by source terms in control volumes in contact with the membrane. The operating

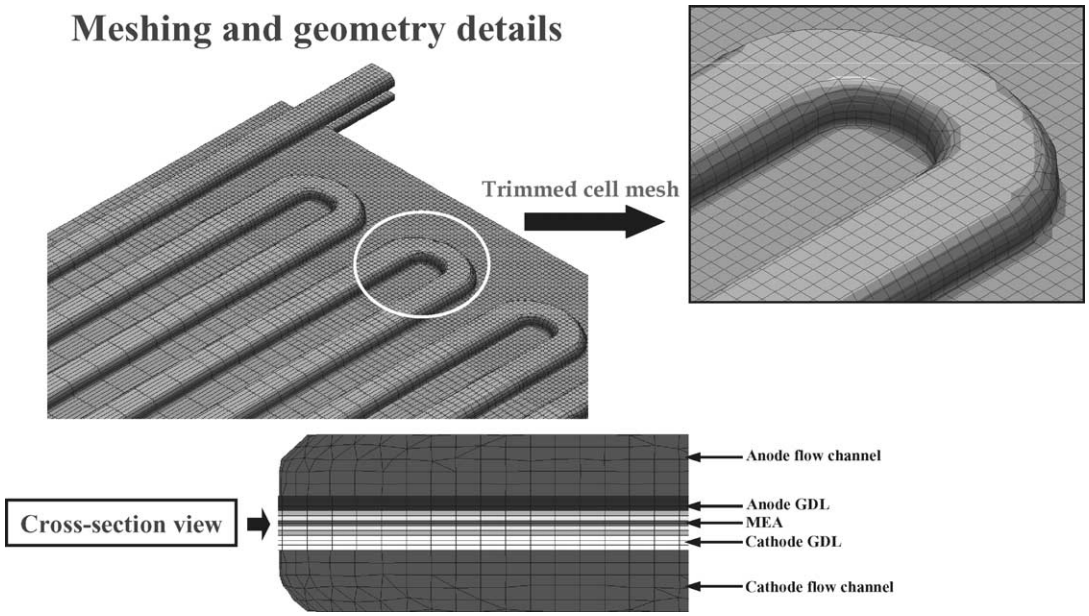


Fig. 2. Detail of geometry at bending channel location showing meshing information to account for curvatures and grid arrangement used in this model.

pressure is one atmosphere and cell temperature is constant at 70 °C. The membrane thickness used in this simulation is 50 μm.

The solution procedure used in this commercial flow solver is based on a SIMPLE algorithm [19] with algebraic multigrid (AMG) method [20,21]. At each iteration, three momentum equations corresponding to three coordinate grids are solved, followed by a pressure correction equation that performs a mass balance. Enthalpy and species transport equations are solved after the bulk flow calculation. The mixture properties at each control volume are calculated based on the local species content. Therefore, the density and viscosity of the mixtures in the anode and cathode flow channels vary from control volume to another.

In order to perform the calculations, STAR-HPC, a parallel solver, was used. STAR-HPC uses a domain decomposition approach to divide the computational geometry among the computational nodes. The computational domains pass information to and from the other domains using MPICH, an open source implementation of the MPI message passing libraries, during iterations, thus the entire domain is solved for. The jobs were run on multiple *x*86 processors running Linux. Fig. 3 details the scalability of the model solution time by comparing the number of iterations per hour for the model as a function of the number of processors used for the computations for an 2.4 GHz Intel Xeon Cluster and Myricom connections for message passing. In terms of CPU time the problem scales logarithmically. Therefore, the number of processor will limit the CPU speed up when a large number of processors are used. Further, message passing and system resources decrease scalability in terms of elapsed time. In this paper, we have not examined the limit of scalability.

Solution convergence is determined by a 1% closure of the global mass and species balances. For this study, all cases were run with constant stoichiometry at a given current. Fixing the current and stoichiometry at given humidification and outlet pressure conditions for a PEMFC yields inlet flow rates and mole fractions for both the anode and cathode. A shoot and correct method is then used to converge on the cell voltage. When a value for the cell voltage is supposed, the model iterates to find the species and electrochemistry distributions. The current from the cell can then be calculated from these distributions and if the current from the cell does not match the current for which the inlet flow rates were set, then the cell voltage is adjusted. The amount of iterations to meet the convergence criteria varies between models and conditions; however, it generally occurs around 600–700 iterations after a change in the cell voltage. At the start of each current condition the model was run for 300 iterations as a non-reacting flow problem for better converge of the mass balance. Generally, it takes around 2000 iterations to run 1 current condition for a model; however, if the cell voltage is well-known, the model could be run in as little as 1000 iterations.

## 3. Results and discussion

To investigate the results for both cases, the overall performance will be presented and then the performance data will be dissected by looking at various electrochemical variables at 0.6 A/cm$^2$ to understand the behavior. Fig. 4 shows polarization curves of both conditions. This figure also shows that in the kinetic region where the cell voltage is high, the dry cathode case performs better than the humidified cathode case. In contrast, as the cell voltage decreases and the

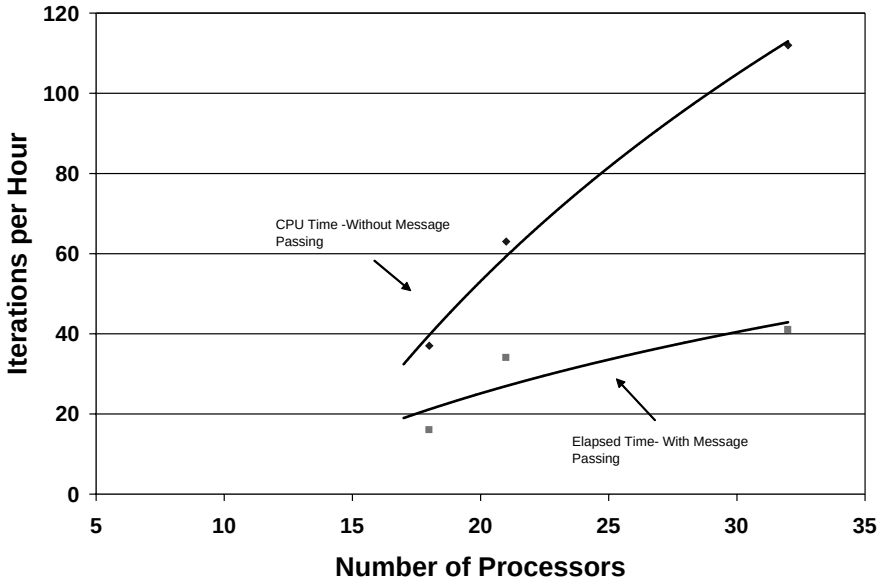


Fig. 3. The parallel computing performance for an Intel Xeon Linux Cluster with Myricom connections for Message Passing.

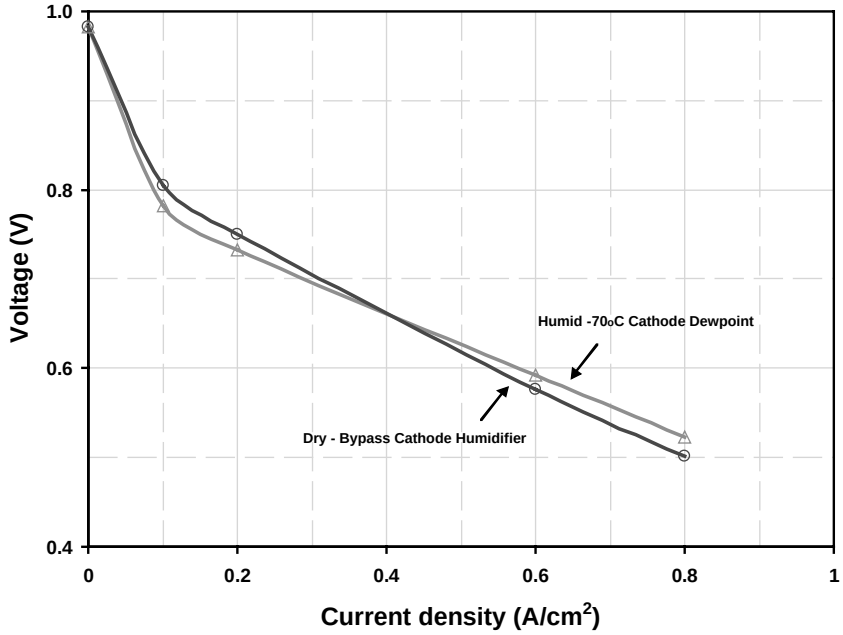


Fig. 4. Comparison of polarization curves between the humidified cathode condition and dry cathode condition ($T_{cell}$ = 70 °C, pressure$(A/C)$ = 101/101 kPa, stoich$(A/C)$ = 1.2 of 40% $H_2$/2.0 of air).

cell begins to operate in the ohmic and mass transfer limited regions, the humidified cathode case performs better than the dry cathode case.

Fig. 5 shows local current density distributions on the MEA surface of both cases. With the same averaged current density of 0.6 A/cm$^2$, the case of humidified cathode gives about 4% higher performance with 0.59 V cell voltage than the dry cathode case with 0.57 V cell voltage. Both conditions have similar current distributions with higher values at the inlet and decreasing values toward the outlet. For the humidified case, the maximum value is 0.97 A/cm$^2$ and the minimum is 0.25 A/cm$^2$. On another hand, for the dry case the maximum value is about 0.8 A/cm$^2$ and the lowest value is 0.40 A/cm$^2$. The humidified cathode condition has a more non-uniform current density distribution than the by-passed cathode at this specific point. Moreover, the current densities at the edges for both cases are very low. This could be due to flooding in those areas, thus the reacting gases have difficulty transporting to the MEA surface.

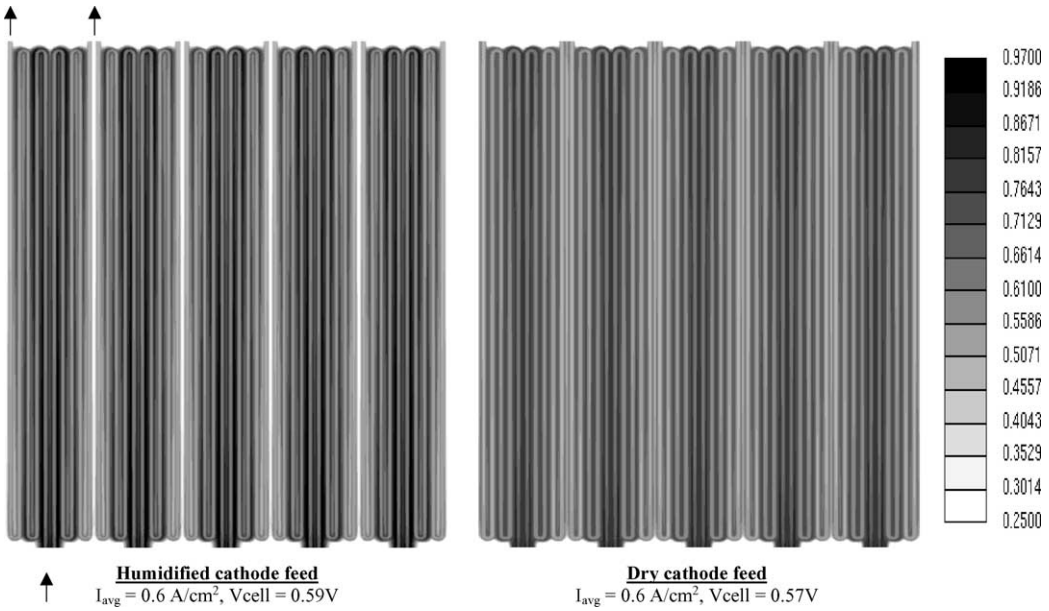


Fig. 5. Current density (A/cm$^2$) distributions on MEA surface at $I_{avg}$ of 0.6 A/cm$^2$ of humidified cathode and dry cathode.

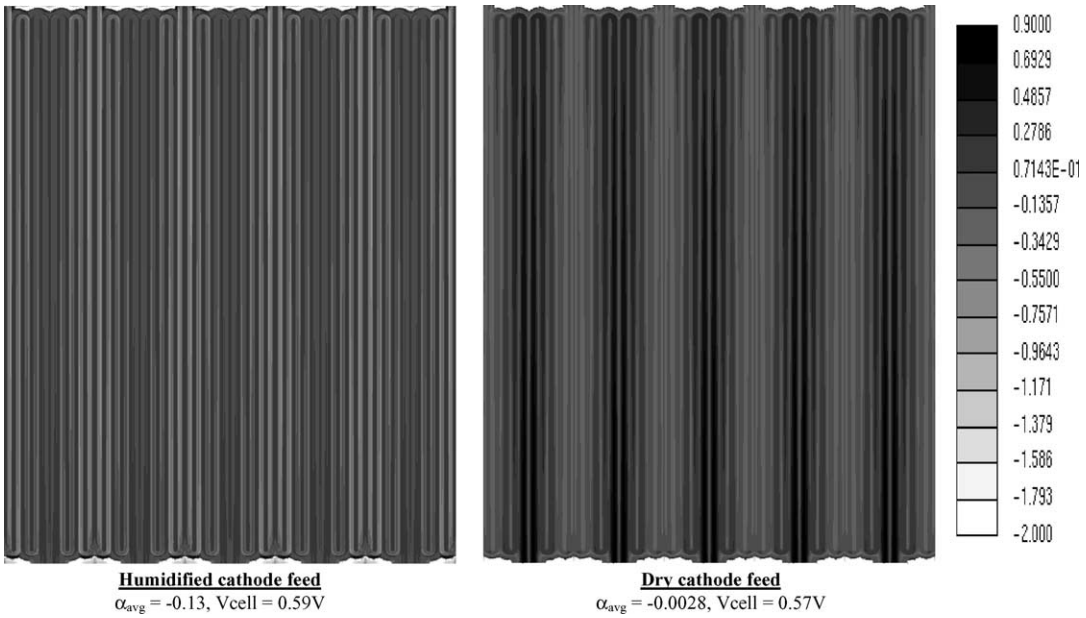


Fig. 6. Net water flux per proton ($\alpha$) distributions on MEA surface at $I_{avg}$ of 0.6 A/cm$^2$ of humidified cathode and dry cathode.

Water transport across the MEA can be described in the form of the water flux per proton ($\alpha$). This variable is a combination of the water dragged electro-osmotically from anode to cathode and the diffusion of water due to concentration gradients across the membrane. Conventionally, $\alpha$ is positive when water is moving from the anode to the cathode and $\alpha$ is negative when water is diffusing from the cathode to the anode. Fig. 6 illustrates the net water flux distributions corresponding to the current density distribution in Fig. 5. Back diffusion of water from the cathode to anode is greatest for the humidified cathode. The highest value of $\alpha$ is a very low positive number of around 0.07 near the inlets and becomes increasingly negative toward the outlets with the lowest value of $-0.8$ and an averaged value of $-0.13$. For the dry cathode, the electro-osmotic drag and water diffusion both drive water toward the cathode from the inlet regions to the center of each segment. After that, water from the cathode diffuses back to the anode in the outlet regions. The value of this coefficient from inlet to outlet is between 0.9 and $-0.35$ with the averaged value of $-0.0028$. This averaged value for the dry case indicates that the membrane is in equilibrium with respect to water transport. Humidification on the cathode side causes more back diffusion than experienced with dry cathode conditions. Again, at the edge of MEA, both cases have highest water back diffusion. The extremely low current density in this region causes little electro-osmotic

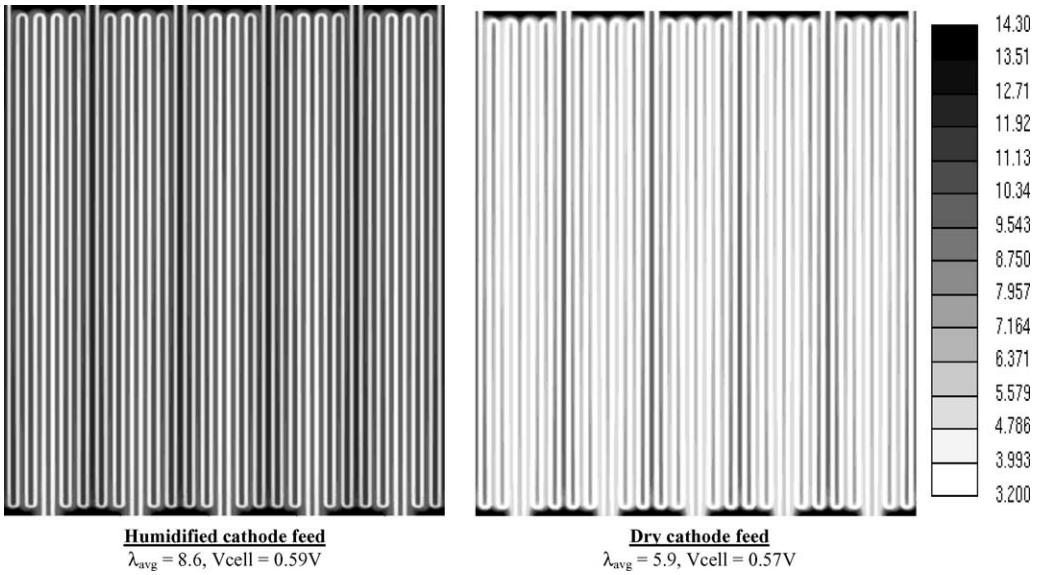


Fig. 7. Water content of membrane ($\lambda$) distributions at $I_{avg}$ of 0.6 A/cm$^2$ of humidified cathode and dry cathode.

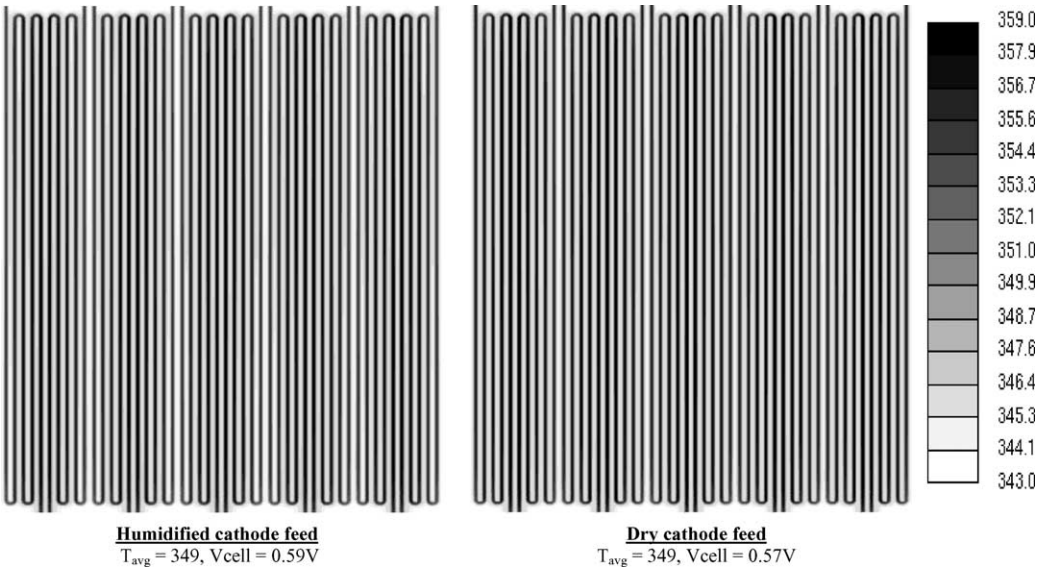


Fig. 8. Temperature (K) distributions on anode MEA surface at $I_{avg}$ of 0.6 A/cm$^2$ of humidified cathode and dry cathode.

drag thus back diffusion is the dominate effect on $\alpha$ in this region.

Another important aspect of water management inside PEMFCs is maintaining adequate membrane hydration. Protons cross the membrane as hydronium ions, therefore, insufficient water in the membrane will decrease the conductivity. Conversely, flooding in the membrane will block the possibility of three phase contact at the electrode MEA interface. The water content of membrane is a good indicator of the membrane hydration state. Fig. 7 shows membrane water content distributions for both operating conditions. The humidified cathode shows significantly higher membrane hydration levels than the dry cathode. For the humidified cathode, the local value of water content increases from inlet toward the outlet due to water back diffusion as explained in Fig. 6. But, for the case of the dry cathode, this value is almost uniform due to the equilibrium of water transport described in Fig. 6. Note that the membrane water content for both cases has a higher value at side-by-side rib-areas than flow channel. This is because the heat transfers from MEA to the top surface of both anode and cathode through rib-area (i.e. bipolar plate) faster than through the flow channel. Therefore, the local temperature of MEA surface is higher at the channel areas when comparing to its

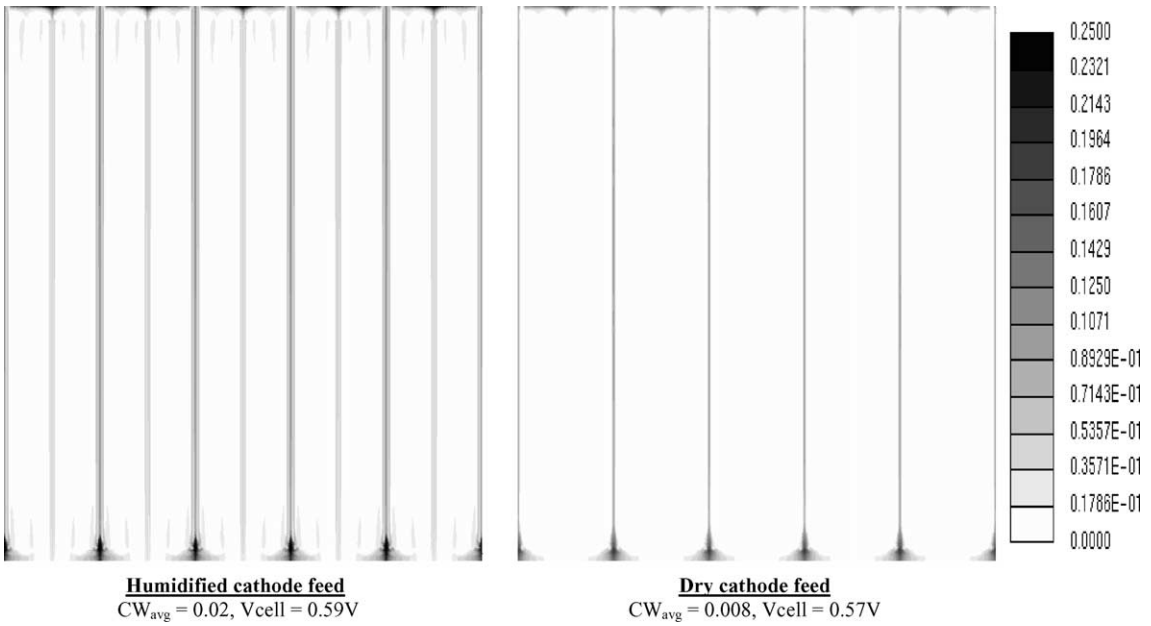


Fig. 9. Liquid water concentration (kg/kg) distributions on cathode MEA surface at $I_{avg}$ of 0.6 A/cm$^2$ of humidified cathode and dry cathode.

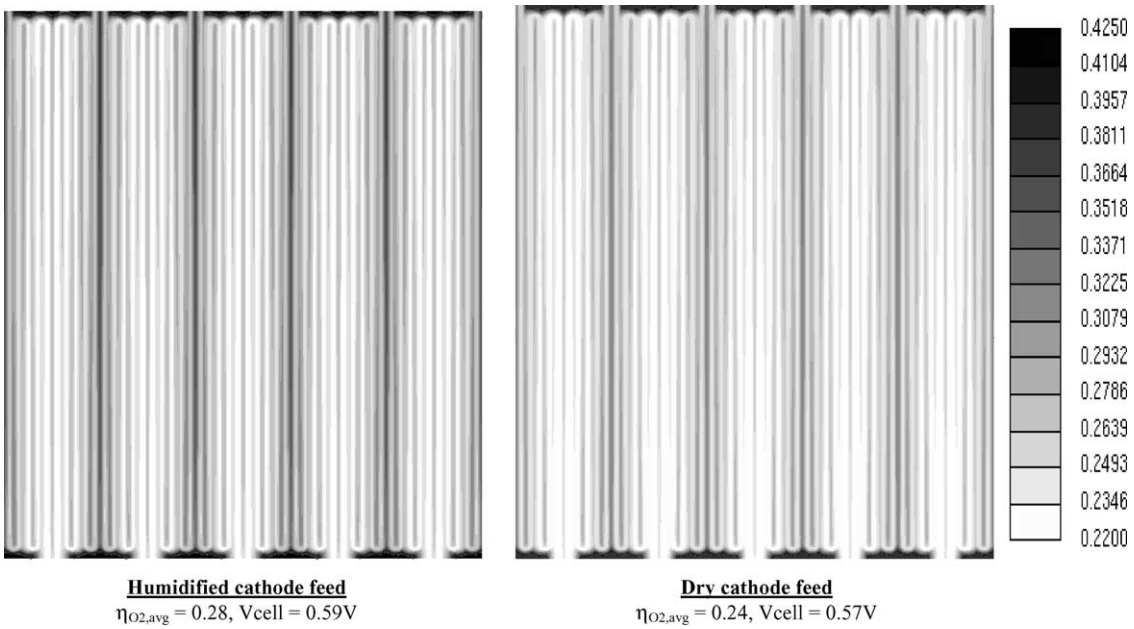


Fig. 10. Cathode over-potential (V) distributions at $I_{avg}$ of 0.6 A/cm$^2$ of humidified cathode and dry cathode.

side-by-side rib-areas as shown in Fig. 8. Again, at the edge of MEA of both cases have high values of water content but the current density is small. This is most likely due to water flooding occurring at both anode and cathode.

Fig. 9 presents the liquid water distributions on the cathode MEA surfaces for both the humidified and dry cathodes. As can be seen from this figure, there is no liquid water present on the cathode MEA surface except flooding at the edge regions where the mass fractions are between 0.07 and 0.25. Therefore, only in these regions does the liquid water resist transport of the reacting gases to the MEA surface thus increasing cathode over-potential as presented in Fig. 10. The local current densities are especially low in these areas. Fig. 10 shows cathode over-potential of both cases. For the humidified case, the over-potential is higher than the dry cathode case from the beginning of inlet flow's location toward the outlet region. This is because inlet water vapor concentration of humidified case reduces the partial pressure of oxygen thus increasing its over-potential.

The advantage of the dry cathode condition, which is appropriate to the operating condition of automotive application, is that pressure drop inside the flow-field is much

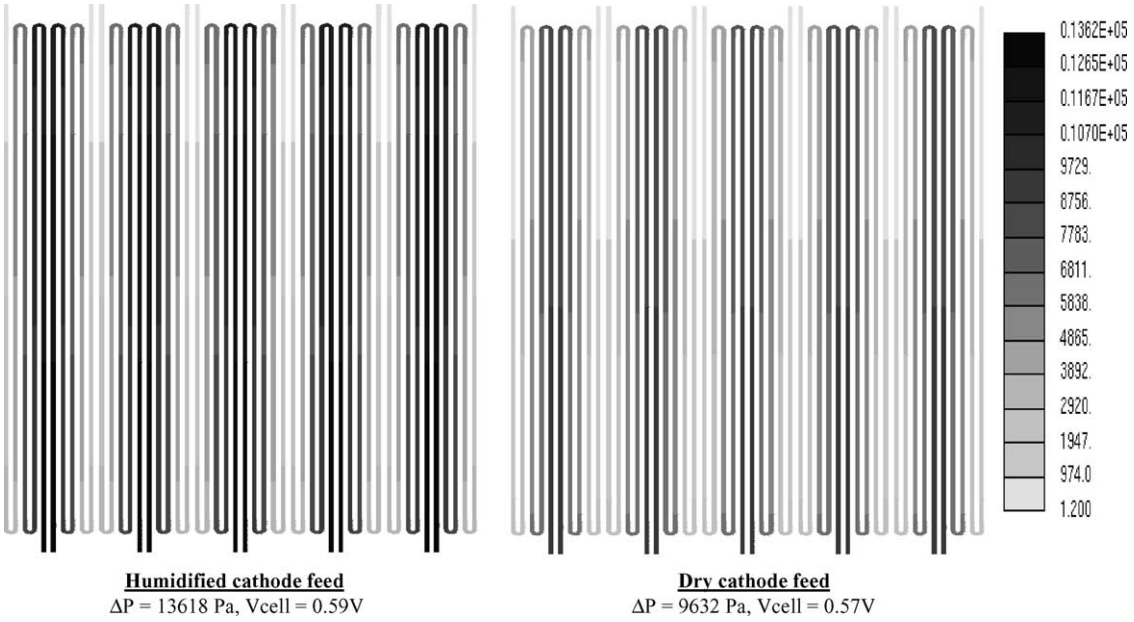


Fig. 11. Relative pressure (Pa) distributions at cathode flow channels at $I_{avg}$ of 0.6 A/cm$^2$ of humidified cathode and dry cathode.

smaller than for the humidified cathode case as given in Fig. 11. For the case of the humidified cathode feed the pressure drop across the cathode flow channel is 13 618 Pa but for the dry cathode feed, the pressure drop reduces 30% to 9632 Pa. This decrease in pressure drop is for a single cell in a stack. Therefore, when cells are stacked together, the humidified case will need more pump power to drive both reacting gas and water especially at the cathode side. Moreover, the pressure build-up inside the cell will not only affect the PEMFC performance but also creates mechanical stresses and strains of bipolar plates, gaskets, GDLs, and MEA.

## 4. Conclusions

Three-dimensional simulation of a large-scale PEMFC has been accomplished using parallel computing techniques. Using the domain composition method, the computational time required for this commercial-size PEMFC was significantly reduced. However, the elapsed time per iteration does not decrease as significantly as the CPU time due to message passing and system requirement. The model presented in this paper could be exercised in 24 h for one data point depending on the number of processors used for the computation.

The patented J.A. Rock flow-field [17] with a symmetric pattern gives uniform distribution without a significant difference in power output between stationary (humidified cathode) and automotive (dry cathode) applications. However, looking at the electrochemical variable distributions gives more insight into the mode of operation. The humidified cathode condition gave higher overall performance than dry conditions even though it performs slightly lower in the kinetic region. This is because membrane dehydration reduces membrane conductivity in the dry cathode feed case that creating a higher ohmic loss across the MEA comparing to the humidified cathode. Even though the dry case has lower cathode over-potential this advantage cannot overcome the lower membrane water content. Therefore, the power output of both cases is not considerably different.

Without humidifying the cathode gas of this flow-field, the pressure drop inside the PEMFC can be reduced by 30% but remain unchanged in performance compared to the case of moistened cathode gas. It is also concluded that with a combination of proper flow-field design and operating condition, this PEMFC can give a high and uniform performance with optimization of water management.

## Acknowledgements

This project was supported by the University of South Carolina and the CD adapco Group.

## References

[1] J. Yi, T. Nguyen, J. Electrochem. Soc. 146 (1999) 38–45.
[2] V. Garua, H. Liu, S. Kakac, J. AIChE 44 (1998) 2410–2422.
[3] A. Kazim, H. Liu, P. Forges, J. Appl. Electrochem. 29 (1999) 1409–1416.
[4] A. Kulikovsky, J. Divisek, A. Kornyshev, J. Electrochem. Soc. 146 (1999) 3981–3991.
[5] H. Naseri-Neshat, S. Shimpalee, S. Dutta, W.K. Lee, J.W. Van Zee, in: Proceedings of the ASME IMECE, vol. 4, Nashville, TN, 1999, p. 341.
[6] S. Shimpalee, S. Dutta, W.K. Lee, J.W. Van Zee, in: Proceedings of the ASME IMECE, vol. 5, Nashville, TN, 1999, p. 464.
[7] S. Dutta, S. Shimpalee, J.W. Van Zee, Int. J. Heat Mass Transfer 44 (11) (2001) 2029–2042.
[8] S. Um, C.Y. Wang, in: Proceedings of the ASME IMECE, vol. 1, Orlando, FL, 2000, p. 19.
[9] T. Zhou, H. Liu, in: Proceedings of the ASME IMECE, vol. 1, Orlando, FL, 2000, p. 43.
[10] S. Shimpalee, S. Dutta, J.W. Van Zee, in: Proceedings of the ASME IMECE, vol. 1, Orlando, FL, 2000, p. 1.
[11] Z.H. Wang, C.Y. Wang, K.S. Chen, J. Power Sour. 94 (2001) 40–50.
[12] T. Berning, D.M. Lu, N. Djilali, J. Power Sour. 106 (2002) 284–294.
[13] S. Shimpalee, S. Dutta, Numerical Heat Transfer-Part A 38 (2000) 111–128.
[14] W.K. Lee, S. Shimpalee, J.W. Van Zee, J. Electrochem. Soc. 150 (2003) A341–A348.
[15] S. Shimpalee, J.W. Van Zee, Int. J. Heat Mass Transfer, submitted for publication.
[16] S. Shimpalee, W.K. Lee, J.W. Van Zee, H. Naseri-Neshat, in: Proceedings of the 01 IECEC, Savannah, GA, 2001.
[17] J.A. Rock, US Patent # 6,099,984.
[18] Gore™ Series 57 MEAs for Transportation Application Brochure.
[19] S.V. Patankar, Numerical Heat Transfer and Fluid Flow, Hemisphere, New York, 1980.
[20] K. Stuben, U. Trottenburg, in: Proceedings of the Conference, Koln-Porz, 23–27 November 1981.
[21] J.W. Ruge, K. Stuben, Frontiers in Applied Mathematics, vol. 5, SIAM, Philadelphia, USA, 1986.